



## OPEN Early stage of metabolic dysfunction associated steatotic liver disease disrupts circadian rhythm and induces neuroinflammation in rats

Paul-Henri Graindorge<sup>1</sup>, Justine Paoli<sup>1</sup>, Berivan Yildirim<sup>1</sup>, Chloe Morel<sup>1</sup>, Ameziane Herzine<sup>2,8</sup>, Maud Collin<sup>3</sup>, Isabelle Gallais<sup>4</sup>, Stephane Boucard<sup>5</sup>, Benoît Pouyatos<sup>5,6</sup>, David Meyre<sup>1</sup>, Dominique Lagadic-Gossmann<sup>4</sup>, Odile Sergent<sup>4</sup>, Henri Schroeder<sup>1</sup> & Nathalie Grova<sup>1,7</sup>✉

Metabolic Dysfunction-Associated Steatotic Liver Disease (MASLD) is a chronic liver disease affecting 25% of the European population, with rising global incidence. Liver damage includes ballooning, steatosis, inflammation and fibrosis. Associated brain disorders include sleep, cognitive issues, anxiety, and depression. While neurological complications in advanced MASLD are well documented, early cerebral manifestations remain largely unexplored. This study aimed at developing an MASLD rat model to assess the onset of early brain damage, focusing on impairments of the circadian cycle rhythm and associated neuroinflammation. Sprague Dawley rats were divided into two groups: one received a high-fat, high-cholesterol (HFHC) diet for 90 days, while the other received a standard diet. Histological analysis showed significant hepatic steatosis, ballooning, and inflammation in the HFHC group ( $p < 0.01$ ). These lesions correlated with elevated hepatic triglycerides ( $p < 0.01$ ), increased Alanine Aminotransferase, Aspartate Aminotransferase, total cholesterol, and low-density lipoprotein, alongside decreased plasma high-density lipoprotein. Behavioural analysis using activity wheels revealed that the HFHC rats steadily maintained their activity level during the rest periods when compared with controls ( $p < 0.05$ ). This behavioural alteration occurred alongside neuroinflammation, demonstrated by changes in the expression of 36 and 17 inflammatory mediators in the cerebellum and frontal cortex respectively. These changes were associated with an increase in the expression of glial cell markers (*Aif1* and *Gfap* genes) and an increase in the number of microglial cells, affecting the frontal cortex and cerebellum differently. This rat model of early MASLD shows circadian rhythm disturbances, which could reflect sleep disorders in humans. These early brain disturbances specific to MASLD, which occur before the symptoms of liver disease become clinically apparent, could therefore be used as an early diagnosis marker for MASLD patients.

**Keywords** Metabolic dysfunction-associated steatotic liver disease, Rat, Neuro-inflammation, Activity impairment

<sup>1</sup>UMR Inserm 1256 nGERE – Lorraine University, 9 Avenue de La Forêt de Haye, 54500 Vandœuvre-Lès-Nancy, France. <sup>2</sup>Plateforme animalerie – Orleans University, 1 Rue de Chartes, 45067 Orléans, France. <sup>3</sup>Animalerie Campus Brabois Santé – Lorraine University, 9 Avenue de La Forêt de Haye, 54500 Vandœuvre-Lès-Nancy, France. <sup>4</sup>IRSET, INSERM UMR\_S 1085, Rennes University & EHESP, 2 Avenue du Professeur Léon Bernard, 35000 Rennes, France. <sup>5</sup>Dept Toxicologie et Biométrie, Institut National de Recherche et de Sécurité pour la prévention des accidents du travail et des maladies professionnelles (INRS), 1 Rue du Morvan, 54519 Vandœuvre-Lès-Nancy, France. <sup>6</sup>DevAH, UR3450, Université de Lorraine – Campus Brabois-Santé, 54519 Vandœuvre-Lès-Nancy, France. <sup>7</sup>UMR Inserm 1256 nGERE University of Lorraine, B.P. 184, 54511 Vandœuvre-Lès-Nancy, Nancy, France. <sup>8</sup>Present address: UMR Inserm 1256 nGERE – Lorraine University, 9 Avenue de La Forêt de Haye, 54500 Vandœuvre-Lès-Nancy, France. ✉email: nathalie.grova@univ-lorraine.fr

**Abbreviations**

MASLD	Metabolic dysfunction-associated steatotic liver disease
HFHC	High-Fat, High-Cholesterol
ALAT	Alanine aminotransferase
ASAT	Aspartate aminotransferase
LDL	Low-density lipoprotein
HDL	High-density lipoprotein
MASH	Metabolic dysfunction-associated steatohepatitis
NAFLD	Nonalcoholic fatty liver disease
ACBS	Animalerie Campus Brabois Santé
CELMEA	Comité d’Ethique Lorrain en Matière d’Expérimentation Animale
APAFIS	Autorisation de Projet utilisant des Animaux à des Fins Scientifiques
E	Percentage of energy
GTT	Glucose Tolerance Test
HOMA-IR	Homeostasis model assessment of insulin resistance
RT-qPCR	Real time quantitative PCR
EEG	Electroencephalogram

Metabolic dysfunction-associated steatotic liver disease (MASLD), is considered one of the major chronic liver diseases in humans, affecting 25% of the European adult population<sup>1</sup>. The incidence of this disease is rising steadily worldwide. Gender differences exist in the prevalence (20.2% in men and 15.8% in women) and severity of MASLD<sup>2</sup>. Although this is true for middle-aged individuals, a recent study has shown that after menopause, the prevalence of MASLD in women becomes comparable to that in men<sup>3</sup>. This metabolic pathology is characterised by accumulating lipids in the liver (> 5% of hepatocytes) not caused by excessive alcohol consumption<sup>4</sup>. The spectrum of MASLD ranges from benign hepatic steatosis to metabolic dysfunction-associated steatohepatitis (MASH), characterised by hepatocyte ballooning, inflammation and steatosis, the most severe forms potentially evolving into fibrosis and even liver cirrhosis and/or hepatocellular carcinoma<sup>1</sup>. In 2023, when the name of the non-alcoholic fatty liver disease (NAFLD) was changed to MASLD by the American Association for the Study of Liver Disease, a set of guidelines was drawn up for investigating the causes of this disease. It has been defined that patients must have at least one of the following five cardiometabolic risk factors: obesity, hyperglycaemia, hypertriglyceridaemia, hypertension and/or a drop in blood levels of high-density lipoprotein (HDL) cholesterol, to be considered as suffering from a MASLD<sup>5</sup>. Insulin resistance, a common cause of liver fat accumulation, may also contribute to the inflammation and hepatocellular damage characterising MASH<sup>6</sup>.

Cerebral damage can occur from the MASH stage of MASLD onwards. Generally, the patients’ cerebral function is affected at the stage of cirrhosis, with the onset of neurological and psychiatric changes, which are part of hepatic encephalopathy. Among the brain disorders emerging from this pathology are sleep disorders, anxiety and depression<sup>7,8</sup>. Signs of impaired executive function and abstract reasoning can also be identified in patients at high risk of hepatic fibrosis<sup>9,10</sup>. Thus, the impact on cognitive performance appears to correlate with the severity of the disease<sup>11</sup>. The MASH stage is reported to have a particular impact on spatial learning and memory<sup>12</sup>. In addition, a certain number of preclinical and clinical studies supported the evidence of cognitive dysfunctions and neuroinflammation in MASH onset<sup>13</sup>.

Sleep disorders, like duration and quality alterations<sup>14</sup>, obstructive sleep apnoea or insomnia<sup>15</sup>, would also be associated with MASLD onset and are therefore considered risk factors in its emergence. The cerebellum is thought to be one of the earliest-affected brain areas, even before the disease reaches the stage of liver cirrhosis. MASH is accompanied by activation of microglia and increased release of pro-inflammatory cytokines in this region<sup>16</sup>. Balzano et al. (2018) demonstrated greater neuronal loss and neuroinflammation in the cerebellum of patients with cirrhosis than in patients with MASH on post-mortem samples, suggesting that the intensity of cerebral damage evolves in parallel with the disease in the liver<sup>16</sup>. This study also highlighted the presence of vascular lesions and the formation of microthrombi in the cerebellum of MASH patients. Moreover, T lymphocyte infiltration of the molecular layer of the cerebellum was revealed<sup>17</sup>. These authors thus concluded that vascular lesions, neuroinflammation and cerebellar degeneration were induced from the MASH stage onwards<sup>16,17</sup>.

The recent study published by Kjærgaard et al. (2024) pointed out an MASLD rodent model assessing early neurological impairments. In this work, the authors showed cognitive disturbances and a depressive-like phenotype in rats fed high cocoa butter and high cholesterol diet for 16 weeks<sup>18</sup>. These impairments observed in the treated rats were associated with the activation of glial cells in the prefrontal cortex<sup>18</sup>. Another study performed in mice submitted to a high-fat diet and the water intake of glucose and fructose for 16 weeks highlighted the association between MASLD and concomitant obesity with anxiety- and depressive-related behaviour and low-grade neuroinflammation. This study also suggested that brain protection from MASLD was caused by the downregulation of the monocarboxylate transporteur-1 Mct1<sup>19</sup>. The link between MASLD and nocturnal/diurnal general activity has never been studied. We have developed a relevant early-stage MASLD rat model based on a high-fat and high-cholesterol diet to mimic the physiopathology of human MASLD and assess the animal’s diurnal and nocturnal activity impairments. The role of neuroinflammation and the expression of genes associated with synaptic plasticity in the development of these deficiencies were both investigated.

## Results and discussion

### HFHC diet triggers gradual MASLD development characterised by mild liver and metabolic alteration

#### Impact of HFHC diet on body weight, liver and visceral fat

At the end of the 30-day diet, the average weight of the HFHC group was significantly below that of the control group ( $p=0.01$ ); which difference was no longer observed at 60 and 90 days (Table 1). This observation indicates slower weight gain during the introduction phase of a high-fat diet compared to the standard diet. Relative liver weight, calculated as the ratio of liver weight to body weight, was significantly higher after 30 days in the HFHC group than in control ( $p<0.0001$ ). Unlike body growth, this difference remained at 60 and 90 days ( $p<0.0001$ ). This suggests that the livers of the rats fed with the HFHC diet reached a state of saturation and fat overload, which did not cease at 60 and 90 days (Table 1).

However, the relative weight of visceral fat did not fluctuate between the 3 stages investigated (Table 1), revealing the constant lack of lipid accumulation in adipose tissue induced by the HFHC diet. This observation aligns with the absence of inter-group body weight differences. These results reveal that our HFHC diet did not

		CONTROL	HFHC	Statistics
Weight parameters				
Weight [g]	30 days	480.2 ± 30.7	436.2 ± 16.7	$p=0.01^*$
	60 days	574.0 ± 47.5	562.6 ± 20.6	$p=0.60$
	90 days	622.9 ± 55.9	632.6 ± 26.9	$p=0.71$
Relative liver weight (ratio of liver weight to body weight)	30 days	3.8 ± 0.2	5.0 ± 0.3	$p<0.0001^{****}$
	60 days	3.4 ± 0.2	4.7 ± 0.3	$p<0.0001^{****}$
	90 days	2.9 ± 0.2	4.5 ± 0.4	$p<0.0001^{****}$
Relative visceral fat weight (ratio of visceral fat weight to body weight)	30 days	1.9 ± 0.2	1.9 ± 0.2	$p=0.61$
	60 days	2.4 ± 0.7	2.8 ± 0.5	$p=0.30$
	90 days	1.9 ± 0.4	1.9 ± 0.4	$p=0.89$
Plasma enzymatic and lipidic profiles				
ALAT [U/L]	30 days	85.3 ± 23.4	84.1 ± 42.5	$p=0.95$
	60 days	68.1 ± 12.5	151.0 ± 94.8	$p=0.06$
	90 days	75.0 ± 15.0	193.3 ± 68.2	$p=0.002^{**}$
ASAT [U/L]	30 days	377.6 ± 99.9	334.8 ± 139.8	$p=0.58$
	60 days	203.3 ± 49.9	334.3 ± 82.7	$p=0.008$
	90 days	193.7 ± 52.2	373.3 ± 104.6	$p=0.003^{**}$
Total cholesterol (mg/dL)	30 days	89.1 ± 20.1	170.8 ± 33.5	$p=0.0004^{****}$
	60 days	88.9 ± 10.3	177.9 ± 14.0	$p<0.0001^{****}$
	90 days	76.8 ± 10.3	124.5 ± 17.5	$p=0.0002^{****}$
HDL cholesterol (mg/dL)	30 days	26.9 ± 5.6	21.4 ± 6.0	$p=0.13$
	60 days	27.1 ± 3.4	19.6 ± 4.1	$p=0.006^{**}$
	90 days	25.9 ± 4.2	18.6 ± 3.6	$p=0.009^{**}$
LDL cholesterol (mg/dL)	30 days	29.4 ± 8.2	94.6 ± 25.0	$p=0.0001$
	60 days	26.4 ± 10.4	110.0 ± 10.8	$p<0.0001^{****}$
	90 days	23.4 ± 4.5	72.5 ± 14.4	$p<0.0001^{****}$
Triglycerides (mg/dL)	30 days	239.1 (208.0–291.8)	227.3 (183.6–287.6)	$p=0.78$
	60 days	238.2 ± 86.4	136.1 ± 40.1	$p=0.03^*$
	90 days	212.8 (162.2–260.0)	115.3 (93.36–131.0)	$p=0.01^*$
Creatinine (µmol/L)	30 days	30.3 (25.75–34.75)	28.1 (26.75–30.0)	$p=0.61$
	60 days	35.3 ± 1.2	32.2 ± 3.0	$p=0.04^*$
	90 days	41.5 ± 2.2	36.2 ± 1.8	$p=0.002^{**}$
Liver lipidic profile				
Total cholesterol (nmol/mg)	90 days	1.9 ± 0.3	26.0 ± 21.0	$p=0.003^{**}$
HDL cholesterol (nmol/mg)	90 days	1.7 ± 0.7	13.1 ± 7.7	$p=0.0004^{****}$
Triglycerides (nmol/mg)	90 days	4.0 (1.85–6.60)	13.1 (6.66–18.41)	$p=0.003^{**}$

**Table 1.** Effects of High-Fat/High-Cholesterol diet on physiological parameters after 30, 60 and 90 days of feeding. Body weight (g), relative liver weight (g), relative visceral fat weight (g), plasma alanine aminotransferase (ALAT) and aspartate aminotransferase (ASAT) activities (U/L), cholesterol (mg/dL), HDL cholesterol (mg/dL), LDL cholesterol (mg/dL), plasma triglycerides (mg/dL), plasma creatinine (µmol/L), liver cholesterol (nmol/mg), HDL cholesterol (nmol/mg), and triglycerides (nmol/mg). Data are expressed as mean ± SD or median (IQR). Unpaired Student t-test or Mann–Whitney test:  $*p<0.05$ ,  $**p<0.01$ ,  $***p<0.001$  compared to control group (n = 5 to 9 per group).

initiate the development of obesity after 90 days of treatment. Our data match those of Maciejewska et al. who demonstrated with a similar rat model that the first changes in weight gain occurred after 120 days<sup>20</sup>. A slight weight increase was observed in another MASLD Sprague Dawley model induced with cocoa butter at 120 days<sup>18</sup>. This 90-day stage perfectly suits behavioural assessment since a significant weight difference between the groups could result in measurement bias rather than treatment-related damage.

#### Liver alterations

Among the four histological criteria investigated on liver sections (lipid droplets, ballooned hepatocytes, inflammatory foci and fibrosis), only fibrosis was not detected in HFHC-group animals, showing an early stage in the development of the hepatic disease. After 30 days of HFHC diet, the rats exhibited the first signs of hepatic steatosis, as indicated by significant rises in the number of steatotic cells (+763%,  $p=0.002$ ), ballooning (+6000%,  $p=0.002$ ), and inflammatory foci (+2 inflammatory foci/field,  $p=0.001$ ) when compared with controls (Figs. 1 and 2a, d, g). This phenomenon increases after 60 diet days, as characterised by higher inflammation (+3 inflammatory foci/field,  $p=0.03$ ). In contrast, ballooning and steatosis remain comparable to the results measured after 30 diet days (Figs. 1 and 2b, e, h). After 90 diet days, the spreads measured between control and HFHC are wider than those recorded previously for ballooning (+2,858%,  $p=0.001$ ) and inflammation (+6 inflammatory foci/field,  $p=0.004$ ), while steatosis remains comparable (Figs. 1 and 2c, f, i). Such hepatic damage is commonly observed in histopathological studies using a similar diet to ours, with variable transitions

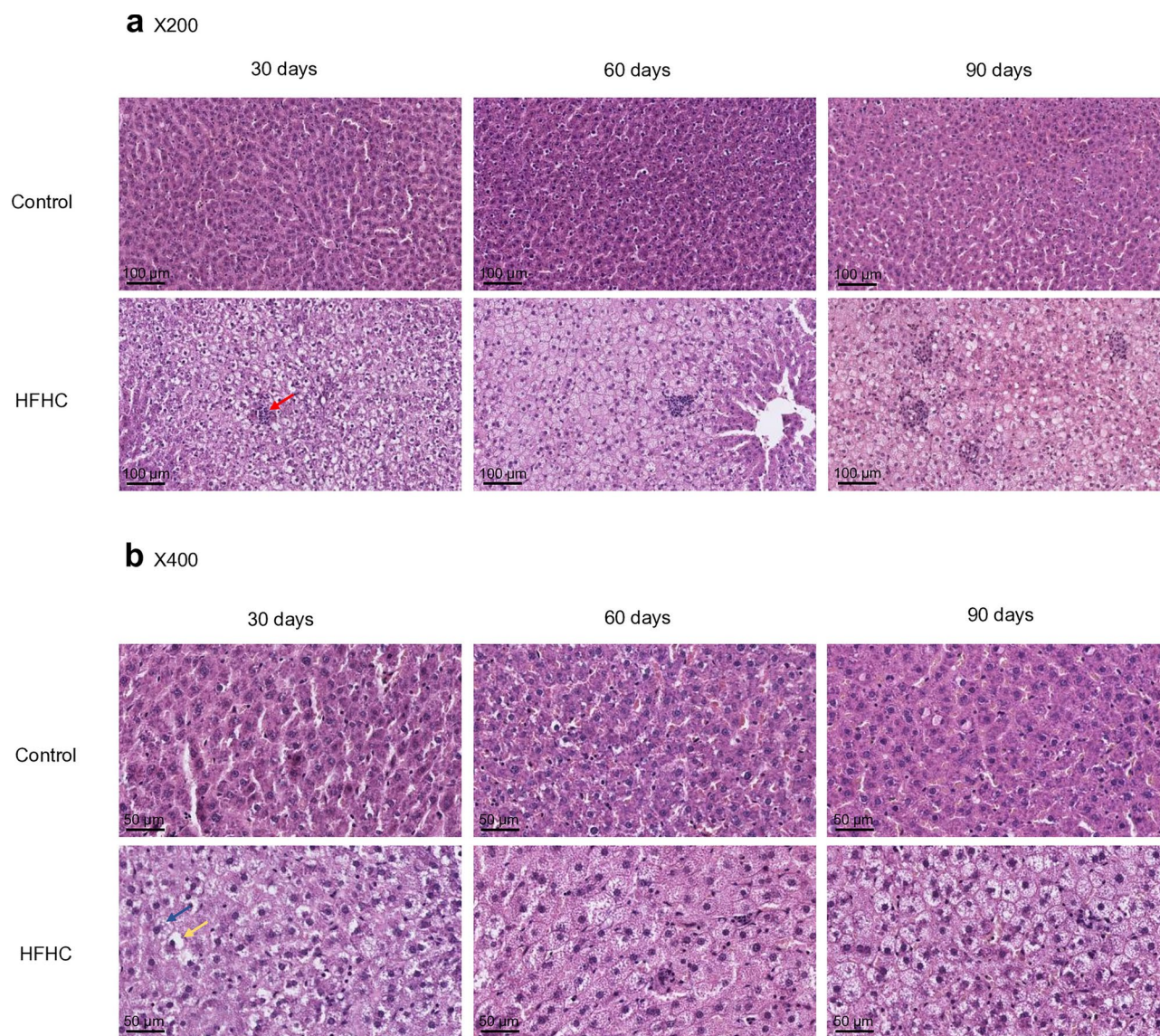


**Fig. 1.** Liver HES-stained sections observed in control animals and High-Fat/High-Cholesterol-fed rats after 30, 60 and 90 days of feeding. Pictures were taken at X200 (inflammation, ) and X400 (ballooning, and steatosis, ).

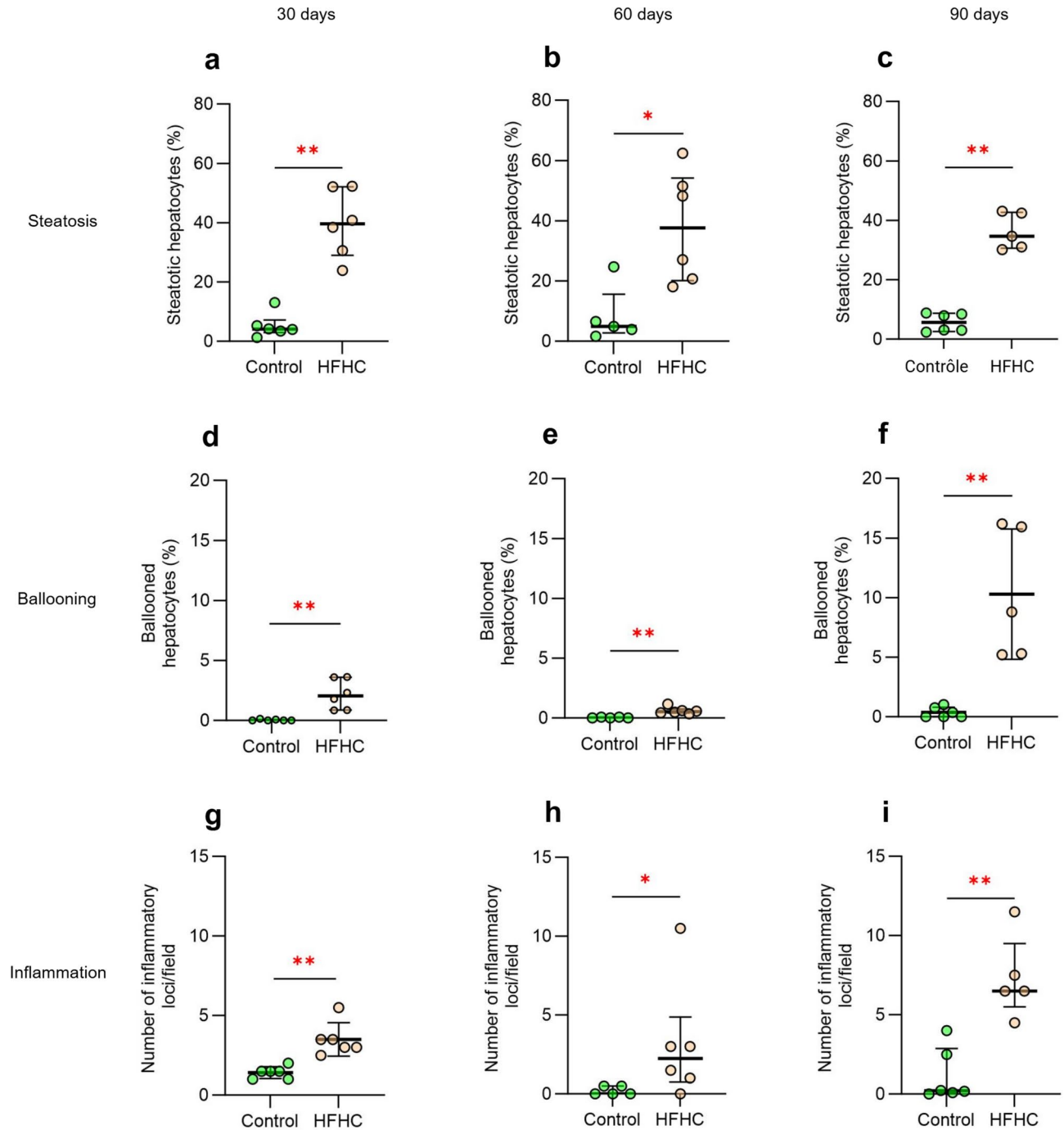


**Fig. 2.** Effects of High-Fat/High-Cholesterol diet on liver histology after 30, 60 and 90 days of feeding. Graphs present results of steatosis at 30 days (a), 60 days (b) and 90 days (c); ballooning at 30 days (d), 60 days (e) and 90 days (f); inflammation at 30 days (g), 60 days (h) and 90 days (i). Data are expressed as mean  $\pm$  SD or median (IQR). Unpaired Student t-test or Mann–Whitney test: \* $p < 0.05$ , \*\* $p < 0.01$  compared to control group (n = 5–6 per group).

to steatohepatitis which may start around 90 diet days<sup>18</sup> or which may still not have occurred after 120 diet days<sup>18</sup>. These differences may come down to different diet compositions and fat percentages.

The HFHC diet did not alter the plasma activities of ALAT and ASAT after 30 days but were respectively 2.2 and 1.6 times higher after 60 days, and of 2.6 and 1.9 times after 90 days (Table 1). The higher activity level of these enzymes indicating cellular alterations, especially hepatocytes for ALAT, is reported in rodent models of hepatic steatosis<sup>20</sup>. Wang et al. (2020) observed similar results with twice higher ALAT and ASAT values than controls in an MASLD model using Sprague–Dawley rats<sup>21</sup>.

Plasma lipid measurements highlighted a higher total cholesterol level after 30, 60 and 90 diet days than controls (Table 1). This increase correlates with a significant reduction in the HDL cholesterol level at 60 and 90 days and a rise in the LDL cholesterol level at 30, 60 and 90 days ( $p < 0.0001$ ). These variations in total cholesterol levels and its lipoproteins attest the emergence of hypercholesterolemia; which confirms the information reported in MASLD rodent models<sup>22</sup>. Concomitantly, the triglyceride rate recorded in the HFHC animals was significantly lower than that observed in controls at 60 and 90 diet days (Table 1). Xu et al. (2010) and Kjærgaard et al. (2024) showed an absence of significant variations in plasma triglyceride levels in adult rats fed high-fat diets for respectively 48 and 16 weeks<sup>18</sup>. To understand this discrepancy, we investigated liver lipid metabolism further by measuring total cholesterol, HDL cholesterol and triglyceride levels. Our data pointed out a significant rise in total cholesterol and its HDL fraction, and in triglycerides in rats fed the HFHC diet for 90 days, in comparison with controls (Table 1). The concomitant increase in triglyceride hepatic concentration and decrease in plasma concentration therefore allows inferring that the HFHC diet induces triglyceride accumulation in the liver. This phenomenon is in line with the study of Donnelly et al. (2005) revealing that MASLD patients exhibited both lower incorporation of food-originating fatty acids into blood triglycerides, and higher incorporation of VLDL-originating fatty acids into hepatic triglycerides<sup>23</sup>.

The significant increase in the expression of 7 hepatic cytokines, namely *Il1 $\beta$*  (4.7-fold increase,  $p = 0.0008$ ), *Tnf $\alpha$*  (3.7-fold increase,  $p = 0.0004$ ), *Ifn $\gamma$*  (87-fold increase,  $p = 0.03$ ), *Cxcl1* (8.3-fold increase, ( $p < 0.001$ ), *Cxcl2* (906-fold increase,  $p = 0.03$ ), *A2m* (1.6-fold increase,  $p = 0.02$ ) and *Nos2* (92-fold increase,  $p = 0.01$ ), further confirms the inflammation occurring in the liver on a molecular level (Fig. 3). Such changes are coherent with the similar model used in the work of Maciejewska and al (2019) in which higher hepatic TNF $\alpha$  levels are observed in HFHC diet-fed animals<sup>20</sup>.

#### Metabolic alteration

The results of the glucose tolerance test, performed after 90 diet days, failed to show significant differences between HFHC and control about fasting blood glucose measured before the administration of the glucose load (T0, Fig. 4a and b), and after 180 min of testing (T180, Fig. 4b). Additionally, the evolution of the blood-glucose curve along the test was not significantly affected by the HFHC diet (Fig. 4a). One should still note the appearance of hypoglycaemia after 60 min, solely in the HFHC group followed by a rebound revealing a second blood-glucose peak after 90 min of testing. The HFHC animals' blood-glucose levels were therefore 10 mg/dL lower than the controls' at 60-min time point. From a kinetic viewpoint, the HFHC group's AUC, Cmax and Tmax values did not differ from the control group's (Fig. 4b), which may be due to the great inter-animal variability in responses. The insulin measurement before the start of the tolerance test did not reveal significant differences between the groups. Likewise, the values of the HOMA-IR index do not vary between the groups (Fig. 4b).

The shape of the HFHC-fed rats' blood-glucose curve does, however, reveal a disruption in blood-glucose regulation, which may be linked to hepatic steatosis and to the metabolic capacity of hepatocytes for glucose. The histological analysis of the pancreas showing hypertrophy of the islets of Langerhans suggests the hypothesis of greater hyperinsulinemia reaction to glucose in the HFHC animals than in controls. Three histological criteria were indeed recorded in the pancreas to enable the assessment of possible damage to the islets of Langerhans caused by the HFHC diet (Fig. 4c). The results showed a substantial increase in the area ( $p = 0.06$ ) (Fig. 4d) and yet another significant increase in diameter ( $p = 0.02$ ) (Fig. 4e) of the islets of Langerhans under the effect of the 90-day HFHC diet. In contrast, the number of islets (Fig. 4f) remained comparable between the groups. This inference seems all the more pertinent as hypoglycaemia reaction to this potential hyperinsulinemia was observed at 60 min in these animals, unlike in controls. In addition, the basal insulinemia values were normal (Fig. 4b), suggesting a dysfunction in blood glucose regulation after feeding possibly indicative of the development of insulin resistance. It is established that diets rich in saturated fatty acids contribute to the development of insulin resistance, unlike mono- and polyunsaturated fatty acids diets<sup>23</sup>. Additionally, these proven disruptions in insulin-induced<sup>24</sup> carbohydrate metabolism were observed for different feeding protocols, different percentages of fat used, and lipids of varying origins<sup>25</sup>. Such alterations were thus reported in rodent models favouring the onset of this comorbidity, for instance the hyperlipidemia model designed in the C57BL/6 mouse fed with a diet containing 60% fat<sup>26</sup>. Besides, many studies have concentrated on carbohydrate metabolism disruptions and insulin in tissues such as skeletal muscle<sup>27</sup> or liver<sup>24</sup>. In contrast, our study was circumscribed to the measurement of circulating glucose and insulin concentrations. Yet, we could not measure insulinemia at any point along the glucose tolerance test.

### Activity impairments, neuroinflammation and expression of genes associated with synaptic plasticity

#### Influence of HFHC diet on locomotor and exploratory activity

The results obtained from the open-field test revealed no significant differences in the total distance travelled and the mobility time of the animals (Table 2). Substantial increases in the number of entries in the peripheral area ( $p < 0.05$ ) and in the central unprotected area ( $p = 0.07$ ) were observed in the HFHC-treated rats upon comparison with controls, whereas the time spent in each zone remained similar between the two groups. These results altogether suggest that the HFHC diet did not impair the locomotor activity of the animals measured in a non-reinforced paradigm for 10 min. The HFHC-exposed rats, however, crossed the peripheral and central areas more often than the control animals, suggesting that they kept their exploratory activity stable, unlike the control rats whose activity levels decreased over the 10-min period of testing. Kjærgaard et al. (2024) reported a slight variation in the anxiety level of the HFHC-fed rats, but no variation in anxiety-related behaviour in a similar rat model of MASLD in 3 different mazes including the open-field<sup>18</sup>.

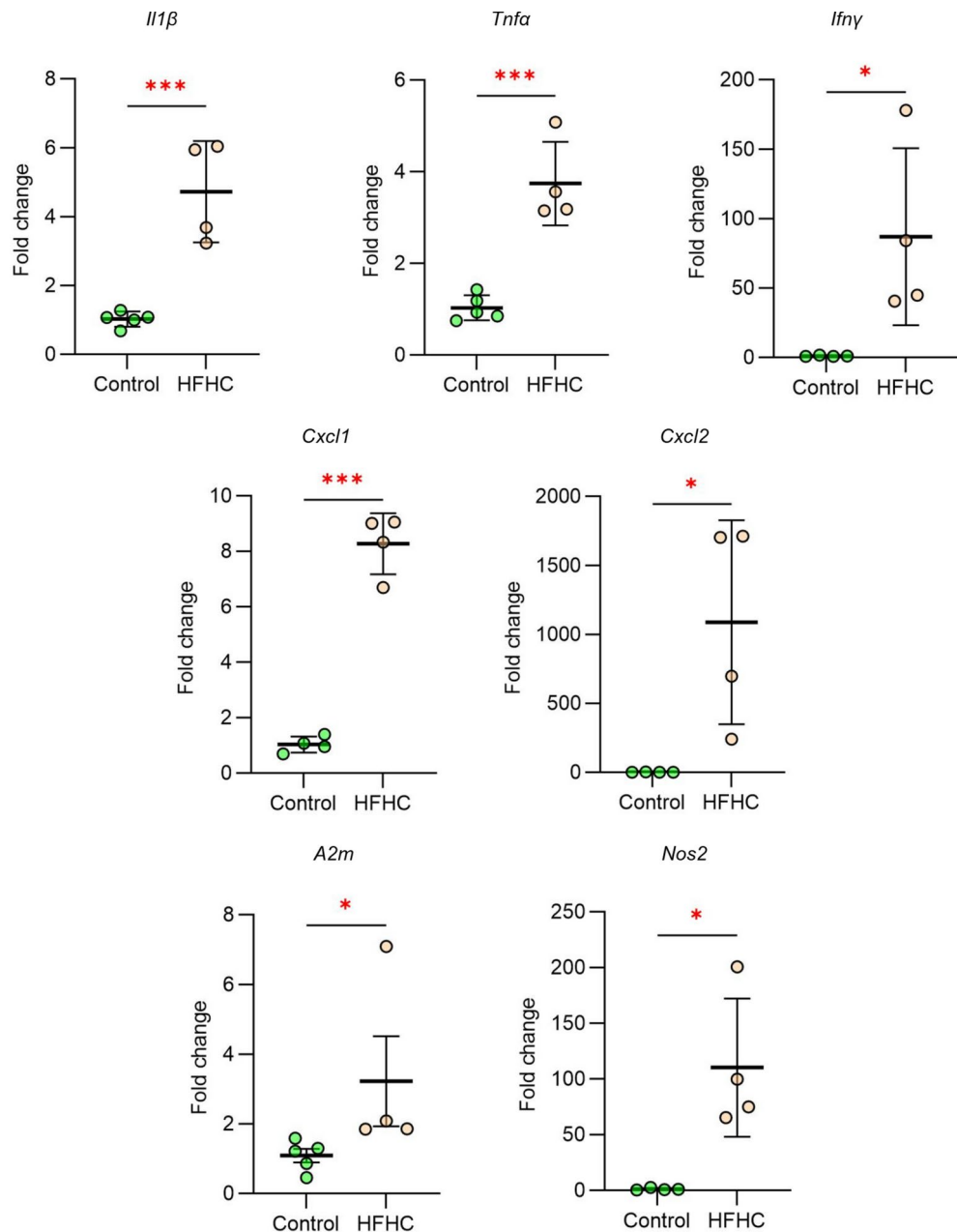


**Fig. 3.** Effects of High-Fat/High-Cholesterol diet on liver cytokines after 90 days of feeding. Graphs present the hepatic expression of *Il1β*, *Tnfa*, *Ifny*, *Cxcl1*, *Cxcl2*, *a2m* and *Nos2*. Data are expressed as mean ± SD or median (IQR). Unpaired Student t-test or Mann–Whitney test: \* $p < 0.05$ , \*\*  $p < 0.01$ , \*\*\*  $p < 0.001$  compared to control group (n = 4–5 per group).

The results obtained in the 3-object-recognition test confirmed the absence of difference in the general locomotor activity level between the two groups. All rats covered the same distance with an increase in the open-field session and the 1<sup>st</sup> trial of the 3-object recognition test, followed by a decrease during the 2 following sessions, still with the same 3 objects aligned (Table S2). Neither spatial nor visual changes of the 3<sup>rd</sup> object induced a similar increase in the time spent exploring the device, thereby demonstrating the absence of cognitive effects of the HFHC diet (Table S2). On the contrary, the rats exposed for a longer period (16 weeks) to the same high-fat diet exhibited a cognitive impairment in a novel object-recognition test<sup>18</sup>. The discrepancy in the anxiety and memory results obtained, when compared to those published by these authors, could result from the difference in the duration of the high-fat diet (12 weeks in our study *versus* 16 weeks in the study of Kjaergaard et al., 2024)<sup>18</sup>.

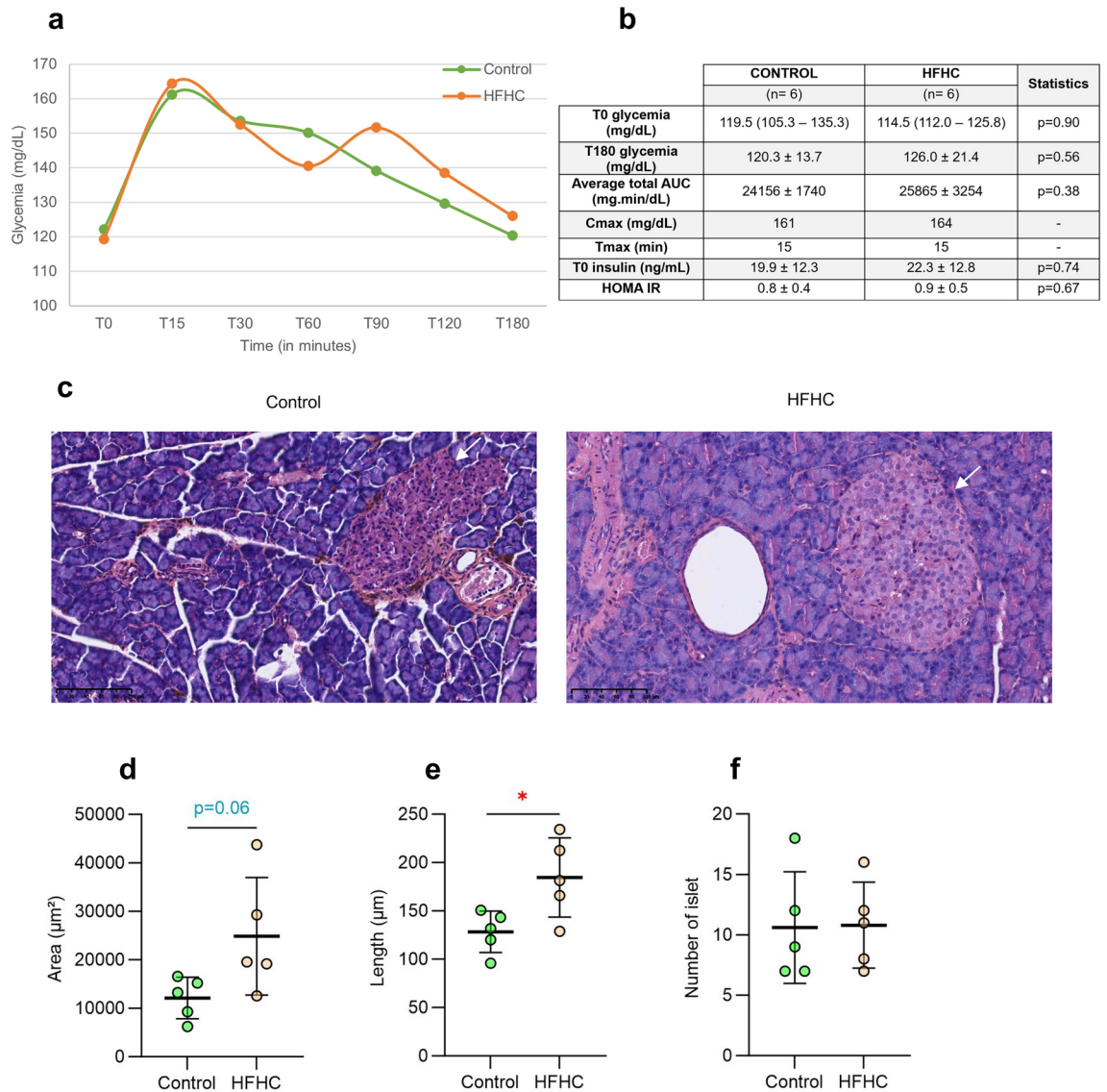


**Fig. 4.** Effects of High-Fat/High-Cholesterol diet on glucose tolerance after 90 days of feeding. **(a)** Glycemia evolution over a 3-h period after a 2 g/kg b.w. oral glucose administration. **(b)** Glycemia kinetic parameters, fasting glycemia and insulin, glycemia measured after 180 min of testing, HOMA IR. Pancreas HES-stained sections images are presented in section **(c)** Graphs present results of area **(d)** and length **(e)** of Langerhans' islets (█). Number of islets is presented in graph **(f)**. Data are presented as mean ± SD. Unpaired Student t-test: \* $p < 0.05$  compared to control group (n=5–6 per group).

#### *Influence of HFHC diet on diurnal and nocturnal activity*

The distances travelled during the first and second 24-h periods proved similar for both groups (respectively, Control:  $43.5 \pm 5.4$  vs. HFHC:  $45.2 \pm 6.5$  m; Control:  $40.4 \pm 5.4$  vs. HFHC:  $39.4 \pm 7.1$  m), suggesting comparable overall activity levels. Similarly, higher activity levels during the two-night phases (red light) than in the diurnal phases (white light) were recorded for both groups without any significant differences in these activity levels. The activity level of the last diurnal phase (from 48 to 60 h) was higher in the HFHC rats than in the controls (Fig. 5a, b), which points to stable activity under the effect of the diet during the last two rest phases. During this last diurnal period, we noted that the HFHC animals had travelled 3 times greater distance than the controls, had activated the wheel 2.6 times as often, and had spent 3 times as long spinning the wheel (Fig. 5c). However, equivalent speed was measured between the groups ( $12.06 \pm 0.53$  Control vs.  $12.4 \pm 0.36$  HFHC revolution/minute), which confirms that the higher distance travelled results from longer time spent in the wheel by the HFHC-group animals. These results can be compared with those obtained in the open field which showed a higher level of exploratory activity (significant increase in the total number, of entry,  $p = 0.05$ ) in the HFHC rats compared to controls, while the level of general locomotor activity remains the same between the 2 groups. Moreover, the expression of the circadian genes *Clock*, *Bmal1*, *Per2* and *Cry1* in the hypothalamus, a key regulator region of circadian rhythm, was studied. Among these 4 genes, only *Clock* was significantly overexpressed in the HFHC

	CONTROL	HFHC	Statistics
Total distance (cm)	4781 ± 1070	5281 ± 711	n.s
Mobile time (s)	346.8 ± 57.9	375.5 ± 43.5	n.s
Total entry	67.5 ± 25.3	89 ± 17	$p = 0.05$
Entries in peripheral area	28.5 ± 9.7	38 ± 6.8	$p = 0.03^*$
Entries in central area	39 ± 15.7	51 ± 10.5	$p = 0.07$
Time in peripheral area (s)	525.6 ± 28.3	509.1 ± 17.6	n.s
Time in central area (s)	74.4 ± 28.3	90.9 ± 17.6	n.s

**Table 2.** Effects of High-Fat/High-Cholesterol diet on anxiety and exploratory behaviours in the open-field test after 90 days of feeding. Data are expressed as mean ± SD. Unpaired Student t-test: \*  $p < 0.05$  (n = 9 per group).

group ( $1.19 \pm 0.18$ -fold change) when compared to the control group ( $1.00 \pm 0.06$ -fold change) (Fig. 5d). While overexpression of the *Clock* gene alone may point to a partial molecular disruption of the circadian rhythm in the hypothalamus, the absence of modifications in the expression of the other genes studied at any given time does not rule out the possibility of altered expression throughout the circadian cycle. This argument can be supported by the work of Yang et al. (2024), who studied the expressions of these circadian genes in the hypothalamus every 4 h over 24 h in a mouse model of repeated inverted light–dark cycles<sup>28</sup>. The results showed that not all circadian rhythm-related gene expressions are altered at the same time.

To summarise, the HFHC treatment does not seem to alter the overall activity level of the animals as measured in the activity wheels during 3 consecutive days. However, the higher-level activity of the HFHC group observed during the second and last 12h-diurnal periods (from 24 to 36 h and 48–60 h of test) suggests an alteration in the activity during rest periods, caused by the diet, and a dysregulation in the day-night cycle-related activity. General or wheel-running activity in facility conditions takes place during the dark phase of the dark–light cycle in nocturnal rodents like rats, with a peak just after the beginning of the dark phase<sup>29</sup>. Several studies have shown association between circadian rhythms and various liver diseases including MASLD<sup>30</sup>, and pointed to the ability of disruptions of rhythms or *clock*-gene expression to participate in liver steatosis and inflammation<sup>31</sup>. In workers, night-shift work positively correlates with abnormal liver function and elevated levels of ALAT<sup>32</sup>.

This alteration of rest-activity may also result from the onset of sleep disorders encountered in humans in the context of MASLD. Additional investigations such as actigraphs or EEG on our rat model could support this hypothesis. Numerous human studies have revealed a link between hepatic steatosis and sleep disorders. A Chinese cohort notably showed that the risk of MASLD decreases along with the increase in sleeping time, especially in men<sup>33</sup>, whereas a Korean cohort<sup>14</sup> reported an opposite correlation. Among the probable causes of this association, the appearance of neuroinflammation may exert a key role. A link between neuroinflammation and a reduction in non-rapid eye movement sleep was recently reported in individuals with and without cognitive disorders<sup>34</sup>. This link does not seem unilateral because several studies have stressed that sleep disorders may also induce neuroinflammation<sup>35</sup>.

The HFHC-fed rats' hyperactivity recorded during the last rest phase could result from the onset of an inflammatory response at the central level. That is why we initially chose to investigate the inflammatory profile in two brain regions: (i) the frontal cortex, known for its role in cognition<sup>36</sup> and sleep regulation in interaction with the hypothalamus<sup>37</sup>, and (ii), the cerebellum, because of its key function in the locomotor activity. This is one of the earliest affected regions by the brain damage linked to the progression of MASLD<sup>16</sup> and its role in sleep regulation has recently been closely investigated<sup>38</sup>. Moreover, circadian rhythms are known to derive from the activity of a central pacemaker located in the hypothalamic area known as the suprachiasmatic nucleus, coordinating circadian rhythms throughout the body by transmitting cyclic signals to other brain regions and peripheral oscillators. Other brain areas, such as the prefrontal cortex and/or cerebellum, exhibit daily oscillations in neuronal activity and can disrupt the rhythmicity of the suprachiasmatic nucleus and/or peripheral oscillators because of their role in most cognitive processes and their sensitivity to disruptions in the biological clock induced by shift work, jet lag, sleep deprivation and/or variations in diet and meal times. Thus, the role of neuroinflammation on the expression of genes associated with synaptic plasticity and nocturnal activity impairments as consequences were investigated.

The response to neuroinflammation was assessed in the cerebellum and frontal cortex by studying the expression of several genes, such as *Aif1* for microglia and *S100b* and *Gfap* for astrocytes. As illustrated by Fig. 6a, the expression of *Aif1* in the cerebellum, was significantly (1.3 times) higher in the HFHC group than in control ( $p = 0.02$ ), thereby reflecting potential microglial activation as is frequently observed in association with neuroinflammation<sup>39</sup>. Besides, the expression of *S100b* was not significantly higher in the HFHC animals than in controls, unlike that of *Gfap*, which was increased by a factor of 3.2 ( $p = 0.003$ ). These results may reveal the existence of an astrocyte reaction concomitant to the microglial activation associated with neuroinflammation. In the frontal cortex of HFHC rats, the expression of *Aif1*, *S100b* and *Gfap* did not show any difference from that in the controls (Fig. 6a). In parallel, the counting of the Iba1-positive microglial cells by immunofluorescence pointed out a significant 1.26-fold compared to controls in the frontal cortex ( $p = 0.03$ ) (Fig. 7a, c) as well as a 1.27-fold increase in the cerebellum ( $p = 0.01$ ) (Fig. 7b, d). Regarding, the measurements of the ramifications, the results between the two groups were similar in the two regions (Fig. 7c, d). A higher number of microglial cells was observed in a similar but more severe murine model, fed a Western diet comprising fatty food consisting

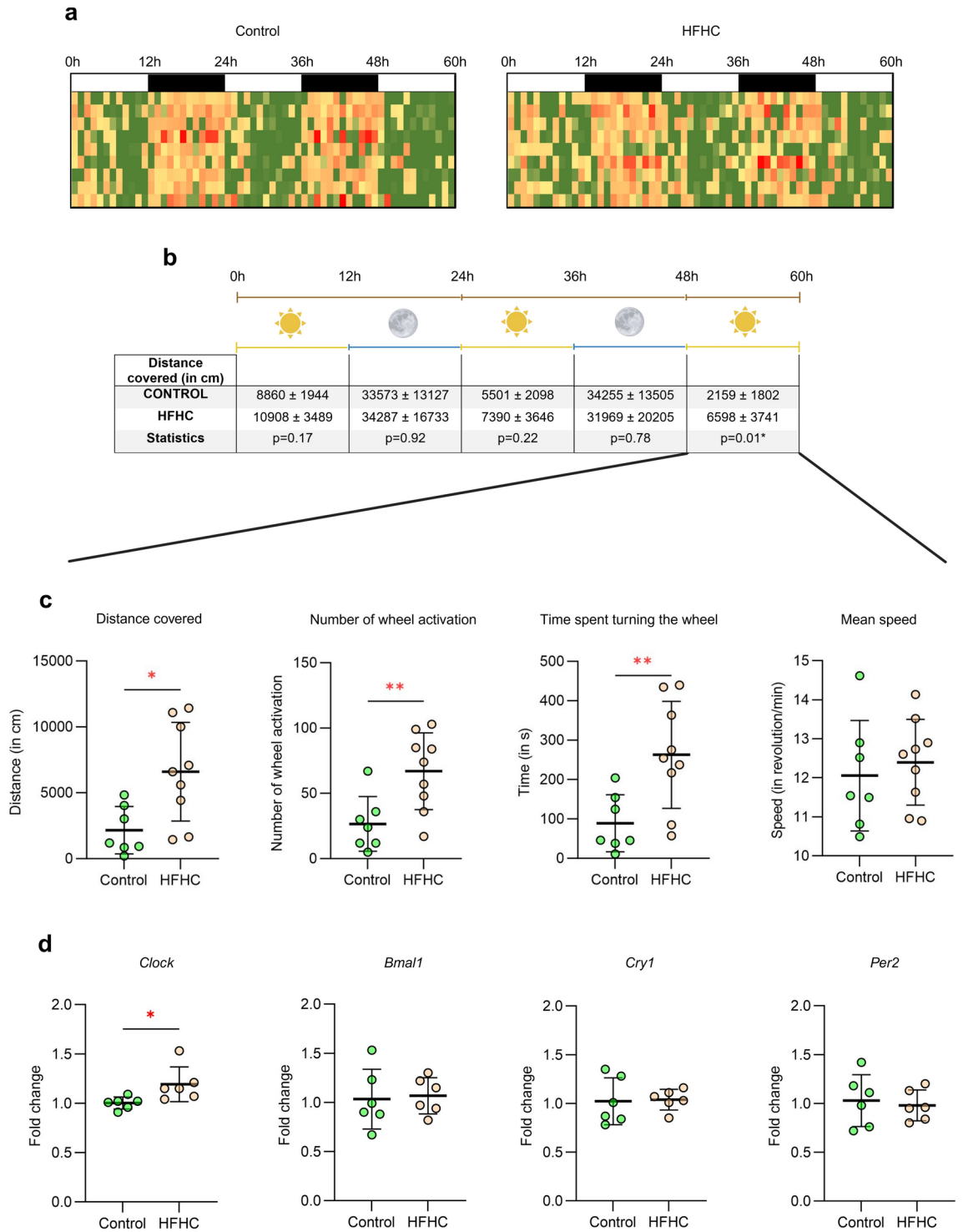


**Fig. 5.** Effects of High-Fat/High-Cholesterol diet on spontaneous activity measured for 2.5 consecutive days in a running wheel apparatus after 90 days of feeding. Actograms (a) show activity levels (red = high, green = low) for each animals over 60 h. The protocol timeline (b) details 12 h with light (☀)/dark (☾) phases. Graphs (c) display distance covered, wheel activations, time spent, and mean speed during the third diurnal period. Data are presented as mean ± SD. Unpaired Student's t-test: \*  $p < 0.05$ , \*\*  $p < 0.01$  compared to control group ( $n = 7-9$  per group).

of 55% lipids and added fructose and glucose in the water for 16 weeks<sup>19</sup>. In this model, which presents a more advanced stage of MASLD, the authors also observed a higher surface fraction of microglial cells and astrocytes<sup>37</sup>. Our results also partially align with those of Balzano et al. (2018), who reported the presence of cerebellar inflammation in MASLD-affected patients, characterised by immune-cell infiltration, and microglial

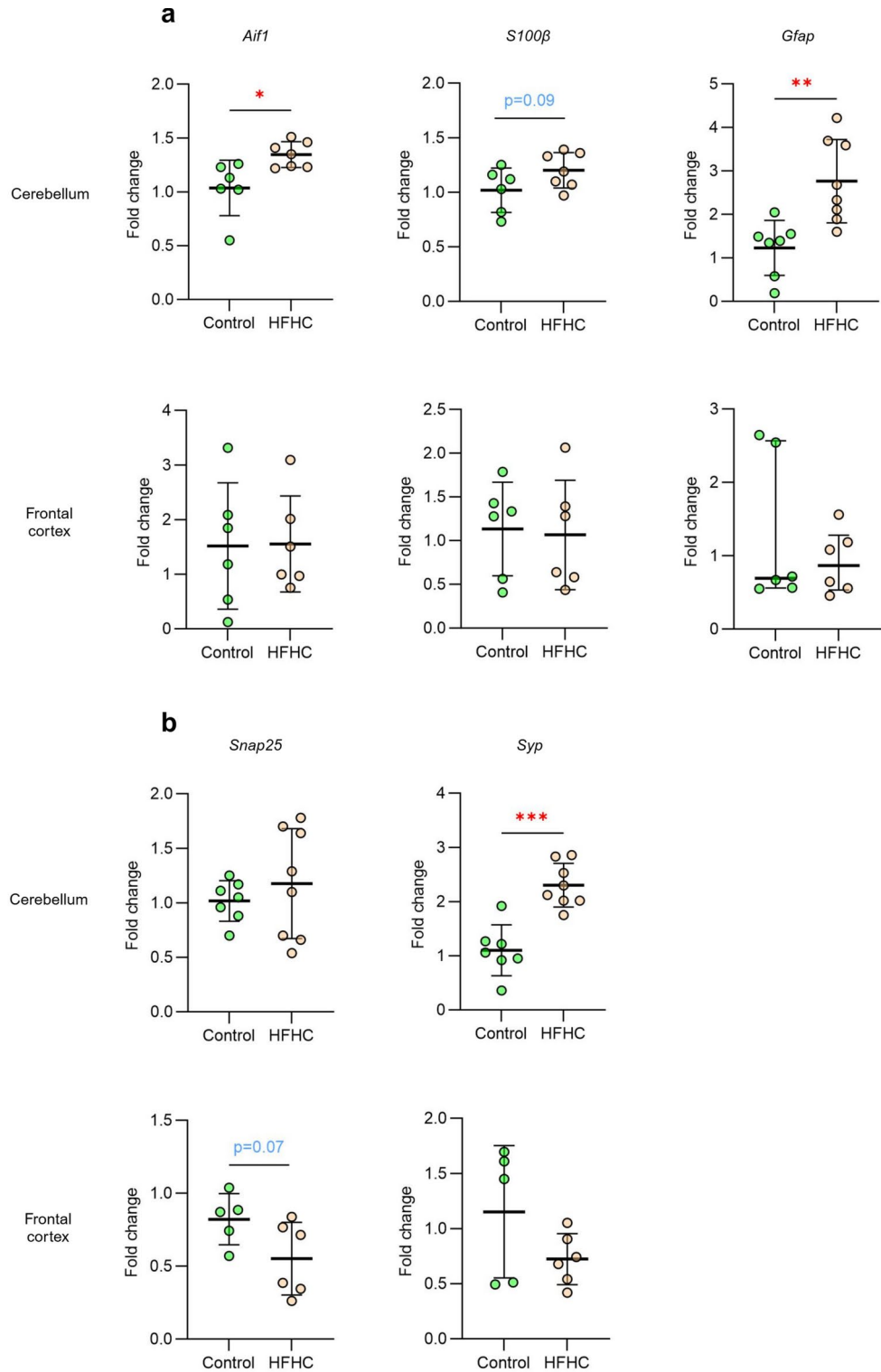


**Fig. 6.** Effects of High-Fat/High-Cholesterol diet on glial cells and synaptic plasticity-related gene expression after 90 days of feeding. Microglia- (*Aif1*), astrocyte- (*S100β* and *Gfap*) related gene expression (a) and synaptic plasticity-related gene expression (*Snap25* and *Syp*) (b). Expression levels were measured in cerebellum and frontal cortex. Data are expressed as mean  $\pm$  SD or median (IQR). Unpaired Student t-test or Mann-Whitney test: \**p* < 0.05 compared to control group (n = 5–9 per group).

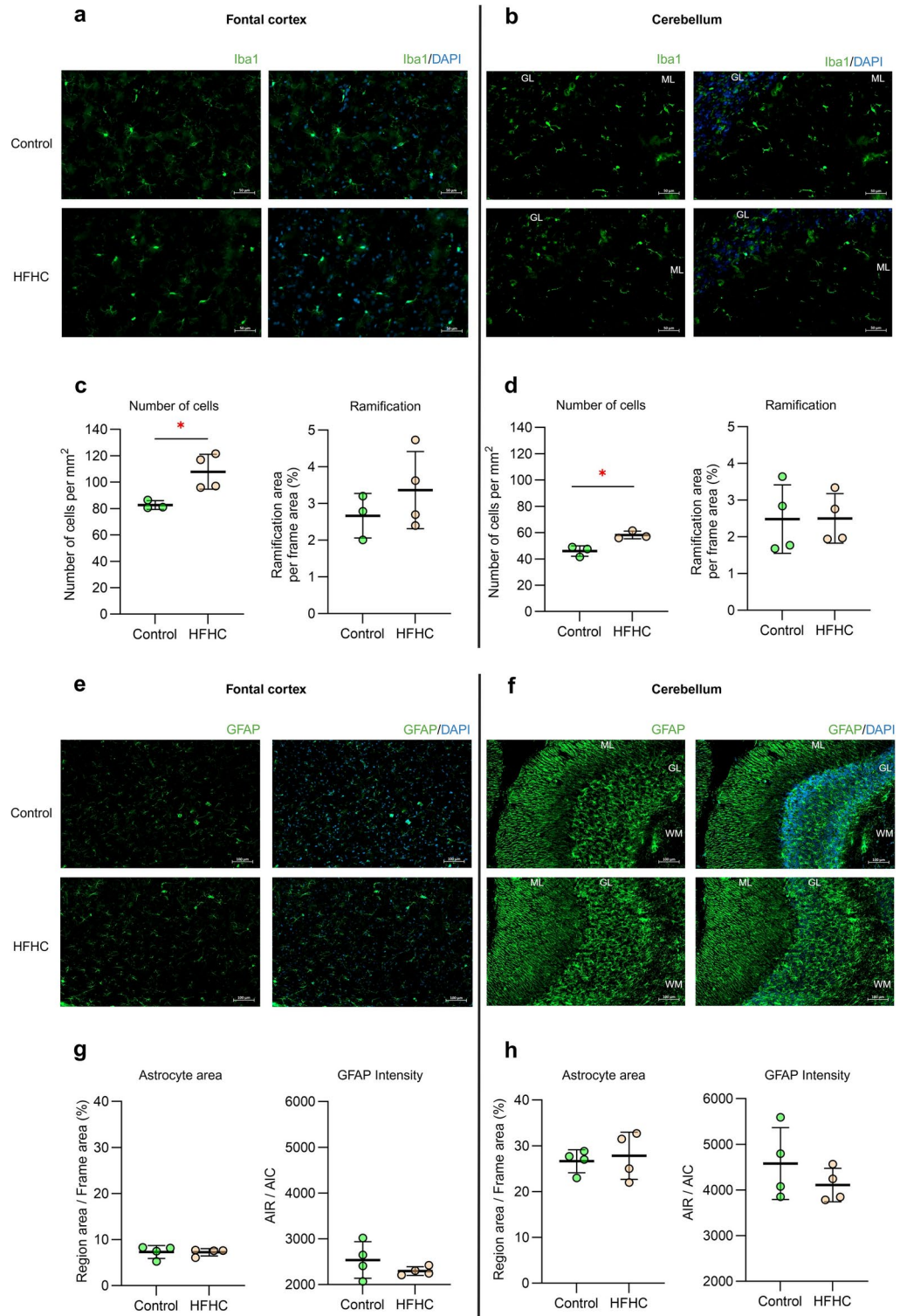


**Fig. 7.** Immunofluorescence staining for microglia and astrocyte in frontal cortex and cerebellum. Representative images (20x) of microglia (Iba1) staining in control group and HFHC group for frontal cortex (a) and cerebellum (b). Number of cellular bodies per mm<sup>2</sup> and total ramification area per frame area of Iba1 stained cells in frontal cortex (c) and cerebellum (d). Representative images (10x) of astrocyte (GFAP) staining in control group and HFHC group for frontal cortex (e) and cerebellum (f). Region areas detected as astrocytes/frame area and Average Intensity per Region (AIR)/Average Intensity value of Channel 'AF488' (AIC) of GFAP stained cells in frontal cortex (g) and cerebellum (h). Data are expressed as mean ± SD or median (IQR). Unpaired Student t-test or Mann–Whitney test: \**p* < 0.05 compared to control group (n = 3–4 per group).

and astrocyte activation<sup>17</sup>. In our HFHC diet model, measurements of the density of astrocytes as well as GFAP intensity did not reveal any differences between the two groups in the frontal cortex and cerebellum (Fig. 7e, f, g, h). This could be due to high interindividual heterogeneity, linked to the initiation of the transition from the inactive to the active form. With regard to this research, the absence of visible astrocyte activation and altered microglial ramification in our model can be attributed to the moderate severity of MASLD in animals fed an HFHC diet.

We then performed a proteome profiler array to assess inflammatory status in the cerebellum and frontal cortex in greater depth. Of the 79 inflammatory mediators detectable by the test used, the results obtained for the cerebellum showed a significant alteration in 36 between the HFHC group and the control group (31 of which being overexpressed, 5 underexpressed). Furthermore, 5 additional mediators showed a statistical trend ( $p < 0.08$ ) towards either over- or under-expression. All in all, 41 inflammatory mediators had their expression modified in the HFHC group, i.e., 52% of the proteins detected. The frontal cortex of the same animals is characterised by the significant overexpression of 10 mediators and 7 more showed a trend towards being overexpressed ( $p < 0.08$ ), with a total of 17 altered mediators representing 22% of the proteins detected (Fig. 8a, b). A total of 7 mediators were overexpressed in both cerebral regions, namely GDF-15, Hepassocin, CCL2/JE/MCP-1, CCL3/CCL4/MIP-1a/B, Lipocalin-2/NGAL, TWEAK/TNFSF12 and IL-3 (Fig. 8c, Table S3).

It has also recently been shown that microglia follow a circadian rhythm, with several markers of immune activation and clock genes periodically expressed without needing immune stimulation. Microglial cells are therefore possibly involved in the regulation of circadian rhythmicity and physiological functions by daily life<sup>40</sup>. This glial cell population is likely to react to sleep deprivation by becoming activated, which is characterised by both a morphological change and an increase in CD11b expression<sup>41</sup>. In response to sleep deprivation, these microglia produce cytokines exhibiting a compensatory mechanism such as IL-1 $\beta$  and TNF $\alpha$ , shown to regulate sleep in sleep deprivation contexts, especially in the cortex. Indeed, these microglial genes are rhythmically expressed with higher levels of expression in day-time than night-time<sup>40</sup>. Our study revealed a significant IL-1 $\beta$  rise in the cerebellum of rats ( $p = 0.002$ ) without alteration in the relative expression of TNF $\alpha$ . In parallel, no difference was noted for these two inflammation mediators in the frontal cortex. The significant increase in the abundance of the TWEAK/TNFSF12 protein in the cerebellum ( $p = 0.009$ ) and substantial increase in frontal cortex ( $p = 0.06$ ) corroborate the potential cellular damage via microglial activation as a compensatory mechanism<sup>42</sup>. This protein belongs to the superfamily of TNF ligands and is capable of binding to the FN14/TWEAK receptor, modulating apoptosis, proliferation and migration of endothelial cells and angiogenesis through this mechanism. This protein, like other members of the TNF ligand family, contributes to the activation, proliferation, differentiation and migration of immune cells in the brain<sup>43</sup>.

The increase in the expression of CX3CL1/Fractalkine in the cerebellum of HFHC rats supports our assumption since its overexpression is indicative of a higher activation level of microglia and its implication in synaptic functionality<sup>44</sup>. Among the growth factors disrupted in HFHC rats' cerebellum, three members of the fibroblast growth factor (FGF) group were over-expressed: FGF-7, FGF acidic and FGF-21. These FGFs are neuroprotective and modulate the differentiation of synapses to become excitatory or inhibitory<sup>45</sup>. IGF-1 is another growth factor involved in numerous brain mechanisms, notably neuroinflammation and synaptic plasticity. The many studies investigating its effects on the brain have reached different and sometimes contradictory conclusions, revealing a context-dependent effect<sup>46</sup>. Its increase in HFHC rats, and the overexpression of IGFBP-2, -3 and -6 in the cerebellum and IGFBP-5 in the frontal cortex, suggests the activation of pro- or anti-inflammatory mechanisms in these regions. It also suggests that a reorganisation of synapses occurs in the cerebellum and possibly in the frontal cortex. Three other growth factors were over-expressed solely in the frontal cortex: SCF and GM-CSF known for their neuroprotective roles<sup>47</sup>, and Endostatin. The overexpression of neurotrophic factors NT-3 and NT-4, particularly in the cerebellum, supports the hypothesis of synaptic modulation, since NT-3 has been shown to increase both the density and length of dendrites, alone or in synergy with IL-1 $\beta$ <sup>48</sup>. Regarding metabolic modulators, fetuin A, which is overexpressed in HFHC rats' cerebellums, is thought to play a neuroprotective role in traumatic brain injury via inhibition of microglia<sup>49</sup>. The increased IL-3 in the cerebellum and CCL11 in both cerebellum and frontal cortex may serve as an indicator of glial cell responses to neurological stress, as both of them can show the influence of astrocytes over microglia in the context of neurological disturbances and have neuroprotective effects<sup>50</sup>. The CNTF increase in the frontal cortex, being neurotrophic and regulating neuro-inflammation, strengthens the hypothesis of a seemingly greater neuroprotective response in the frontal cortex. However, lipocalin-2, a protein secreted by activated astrocytes promoting neuro-inflammation<sup>51</sup>, is overexpressed in both the cerebellum and frontal cortex of HFHC-fed rats, which further demonstrates the complexity of the immune response in those regions.

The various pro-/anti-inflammatory mechanisms impacted at central level associated with modified expression of genes associated with synaptic plasticity suggest an immune and physiological response of the brain to the stress triggered by the HFHC diet at the same time as liver damage. These perturbations could then interfere with the rhythmic expression of the circadian genes and disrupt the day-night cycle, as observed in HFHC rats in the running wheel activity task. These alterations would differ between cerebellum and frontal cortex. Gene-expression analyses of *Syp* (coding for synaptophysin) and *Snap25* were then performed to support the hypothesis of impaired synaptic connectivity and/or plasticity. The analysis of the expression of these genes in the cerebellum revealed a twofold increase in synaptophysin gene expression in the HFHC group. However, no significant inter-group differences were recorded regarding *Snap25* gene expression (Fig. 6b). Thus, in the cerebellum, synaptic connectivity and/or plasticity might be affected by disrupted neurotransmitter release at the pre-synaptic level, potentially caused by the HFHC diet. A different expression profile is recorded in the frontal cortex for both genes. We indeed observe a trend towards a 1.5-fold reduction in *Snap25* ( $p = 0.07$ ) in the HFHC group, correlating with similar *Syp* expression between the two groups (Fig. 6b). This observation suggests that neurotransmission in this brain structure could also be affected by disruptions in the re-uptake

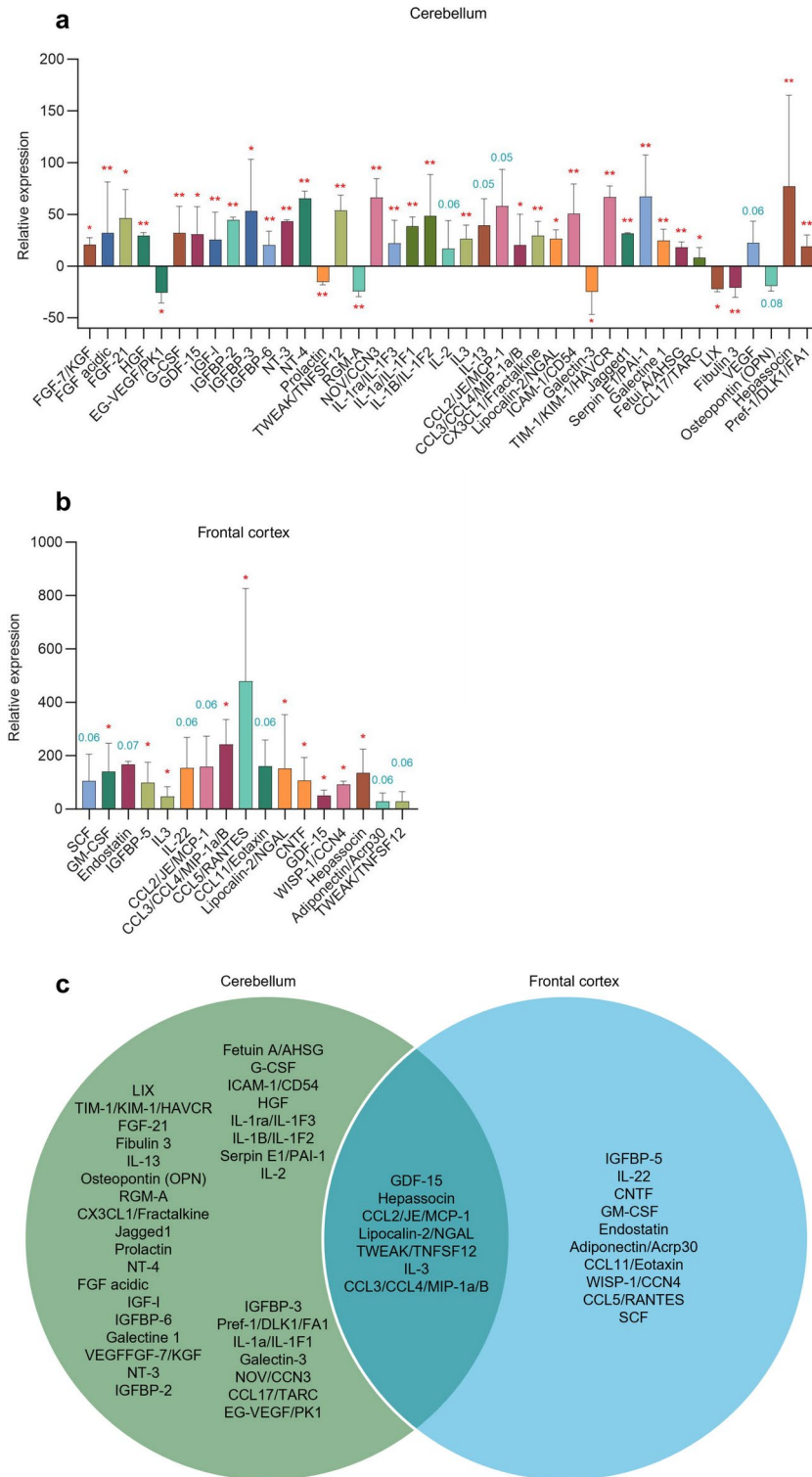


**Fig. 8.** Relative expression of inflammatory mediators referred to control values in the cerebellum and frontal cortex of High-Fat/High-Cholesterol-fed rats after 90 days of feeding. Data are expressed as median (IQR). Mann–Whitney test: \* $p < 0.05$  compared to control group ( $n = 4-6$  per group).

process at the pre-synaptic level. Reductions in the expression of *Snap25* in the cortical zone<sup>52</sup> were previously noted in sleep-deprivation contexts.

## Conclusion

In this study, we developed a Sprague Dawley rat model adapted to monitor the progressive onset of MASLD by analysing blood and liver histopathological markers. This model enabled us to demonstrate the onset of behavioural disorders at an early stage of the disease, after 90 days of high-fat diet, marked by a disturbance in diurnal (resting period) activity and associated with neuroinflammation and increased number of microglial cells affecting the cerebellum and frontal cortex differentially. To confirm that the quantity and quality of sleep are affected in our model, its analysis by EEG would be relevant and appropriate. This rat model of early MASLD shows circadian disturbances, which could reflect sleep disorders in humans. These early brain disturbances specific to MASLD, which occur before the symptoms of liver disease become clinically apparent, could therefore be used as an early diagnosis marker for MASLD patients.

## Material and methods

All the animal experiments were conducted according to the European Union directive (2010/63/EU). The experimental protocol was approved by the institutional ethics committee of Lorraine University (CELMEA n°66) and authorized by the French National Consultative Ethics Committee (APAFIS #35584-2022040415433064 v3). The study is detailed in accordance with ARRIVE guidelines and recommendations.

### Animal experimental design

Our objective was to reach an early stage of the disease in a progressive and slow manner, as observed in humans. For this reason, diets based on high concentrations of lipids and on the addition of sugars were excluded, as were diets deficient in methionine and choline. Our model is based on the work of Maciejewska, D et al. (2019) which chose bacon as fat type, due to its high content in saturated fatty acids; the latter accounting for 30% of the energy provided by the diet (a fairly low concentration compared with the 45–60% often observed in the literature)<sup>20</sup>. We also chose to include an additional 2 g of cholesterol per 100 g of food, as this appears to promote liver damage, something that hyperlipidic diets alone do not always achieve. The isocaloric administration of the diet, set at 21 kcal/100g b.w./day, allowed us to control the food intake in that this diet was likely to be more palatable. In addition to this aspect, we obtained a non-obesogenic model that made it possible for us to focus on hepatic and cerebral alterations. This thereby eliminated the possible harmful effects that a generalised lipid overload directly linked to obesity could exert, while also avoiding the biases in terms of behavioural assessment linked to overweight. Due to higher prevalence of MASLD in males than in females which tends to increase along with age, we selected male Sprague–Dawley rats at young adult stage.

Five-week-old male Sprague–Dawley rats (RjHan:SD, n=54) were purchased from Janvier Labs (Genest-Saint-Isle, France). After a one-week acclimatisation period prior to the start of the experimental protocol, the animals were randomly pair-housed in plastic isolator cages on a ventilated rack (Techniplast, Grostenquin, France), in the specific pathogen-free sector of the animal facility (ACBS, authorization number C5454730). They were kept under a 12 h/12 h reversed light cycle (red light on at 7.30 a.m.; white light on at 7.30 pm) at 22°C ± 2°C and relative humidity of 55% ± 10%. Access to food was free but controlled in quantity, and water was supplied ad libitum. The animals were randomly divided into batches of 12 over 2 feeding periods (30 and 60 days) and a batch of 30 for a third feeding period of 90 days, according to the following experimental groups: the control group (standard diet, A04 SAFE, Rosenberg, Germany) and the HFHC group (High Fat High Cholesterol diet supplied by SAFE). Figure S1 (supplemental data) displays the sample size of the animal protocol. The HFHC diet composition was assessed by Agrolab (Kiel, Germany): the percentage of energy (E) brought by carbohydrates was 52.3% E, by fat 33.7% E and by protein 13.9% E instead of respectively 72.4% E, 8.36% E and 19.3% E for A04. The percentage of fibre was similar between both diets (3.8% for HFHC vs 3.7% for A04). Supplementation in cholesterol (2.07 g/100g of food) and methionine (0.27 g/100g of food) in the HFHC diet was validated.

### Glucose tolerance test (GTT)

The animals were fasted for 12 h before the GTT. On test day, the rats were placed in an incubator set at 37.5 °C for dilation of the tail veins. The rats were then placed in a restraint tube, and a catheter (24G, Terumo) was inserted in one of the lateral tail veins for 3 h. Before glucose administration, 125 µL of blood were collected (in a 500 µL EDTA K2 collection tube) and fasting blood glucose was measured using a blood glucose meter (Accu-Chek, Mannheim, Germany). Each rat received an equivalent 2 g/kg bw glucose volume by oral gavage. Blood (125 µL) was collected at 15-, 30-, 60-, 90-, 120- and 180 min post-gavage, and blood glucose measured at each timepoint. Plasma insulin at T0 was measured by a Rat Insulin ELISA kit (Proteintech, Manchester, UK) and analysed by absorbance measurement using a SpectraMax iD3 instrument (Molecular Devices, San José, California, USA) at 450 nm. HOMA IR was calculated using the following formula:  $IR = [FI (\mu IU/mL) \times FBG (mmol/L)] / 22.5$ .

### Behavioural assessment

Behavioural investigation was performed on the same animals for each test (n=9 per group). The open-field test consists in assessing the spontaneous locomotor activity of an animal in the maze. From its initial position at the centre of a one-hundred cm-wide circular wall (Intellibio Innovation, Nancy, France), the animal is left to explore the enclosure freely for 10 min. The “protected” peripheral zone was defined with a distance of 16.5 cm between the outer edge of the open field and the boundary of the “open” central zone, which itself had a diameter

of 67 cm. The variables recorded (distance covered, number of entries in the peripheral or central areas) allow the evaluation of the animal's locomotor activity level and the exploration activity of both areas according to how protected these areas were. The test was performed between 7:00 and 10:00 am on the 79th day, in red-light conditions (13 lx). Each rat was initially placed at the centre of the device. Videorecording and analysis were performed with Anymaze software (Dublin, Ireland).

We assessed the cognitive performances of the rats in a 3-object recognition test at the end of the 90-day dietary period. This object-recognition task is a non-rewarding paradigm based on the spontaneous exploratory behaviour of the rats whose motor activity, habituation to the test environment, and responses to both spatial rearrangement of familiar objects and object novelty are measured.

The apparatus used for the study consisted of a circular open-field device, 1m in diameter that the rats were allowed to explore freely for 10 min at each session. The rats were tested for 4 consecutive days, with one session at days 1 and 2, and two consecutive sessions at days 3 and 4. All the tests were performed under red dim light and recorded using ANYMAZE software (Dublin, Ireland). A 280 cm<sup>2</sup>-area (18.90 cm diameter) around each object was delineated and the exploring time spent by the rats was measured over each 10 min session of testing. At the start of the test (day 1), each rat was placed in the centre of the device and was left free to explore the enclosure for 10 min. On the second day, three identical metallic objects (silver door wedges, 7 cm high and 5 cm in diameter) were aligned in the central part of the open field. The distance between the objects was 6.90 cm with the middle one placed at the centre of the apparatus. The comparatively high weight of each object did not allow the rat to displace them. The animals were allowed to explore the maze and the 3 objects freely for 10 min, which enabled them to get used to memorising both the colours and spatial positions of the objects.

On the third day of testing, the animals first underwent a 10-min session identical to the one performed the day before. Thirty minutes later, each rat was tested for 10 min in the presence of the 3 objects, with one being displaced 90° from its initial position (object 3, see Fig S2). This move made it possible to study the ability of the rats to detect the changes in the spatial arrangement of the objects, therefore providing an indicator of their behavioural flexibility in the face of spatial changes in the environment.

On the fourth day of testing, the session carried out on the second day and the first session of the third day was repeated for 10 min. Thirty minutes later, the rats were assessed for their behavioural performances for 10 min in the presence of the 3 aligned objects but with the third one being placed at the end of the line replaced with an object of the same type but of a different colour. The aim of this task was to study the visual recognition and selective attention of the rats towards a new distinct stimulus. It was also used to assess their short-term memory, their ability to adapt to a perceptual change and their preference for a novel object over familiar ones.

The activity wheels (Intellibio Innovation, Nancy, France) were used to measure rodents' free and spontaneous activity in their cages. Activity was measured in real-time in a cage equipped with a wheel connected to the ActiviWheel software (Intellibio Innovation, Nancy, France) for data-recording. The variables recorded were the distance covered, the time spent in the wheel, the number of wheel activation and the mean speed. The animals were placed individually in the cages fitted with the activity wheels for 72 h during which spontaneous activity was continuously measured between the 70th and 73rd days of the protocol. The animals were placed in the apparatus at the beginning of the first 12-h nocturnal cycle, which served as a habituation phase and was not recorded.

### Blood and tissue sampling

After 30, 60 and 90 days of exposure, all animals were euthanised by CO<sub>2</sub> inhalation. Blood samples were collected in EDTA K2 tube by intracardiac puncture using an 18G needle. The blood was centrifuged at 2500 g for 15 min for plasma isolation; then again extemporaneously at 2500 g for 15 min for platelet-free plasma collection. The plasma was used for enzymatic and lipidic biochemical analysis. A lobe of the liver and the tail of the pancreas were collected, fixed in 4% paraformaldehyde for 48 h, and placed in paraffine for histological studies. The brain was dissected, and the hemispheres were separated for the collection of the frontal cortex and cerebellum. Visceral fat was collected and weighed to allow the investigation of the HFHC-diet-induced weight gain pattern. The technical details and protocols regarding enzymatic and lipidic profiles, hepatic and pancreatic histology, gene expression (RT-qPCR), proteome profiler cytokine array and analysis by immunofluorescent staining of frontal cortex and cerebellum are detailed in supplemental data.

### Statistical analysis

Normality was assessed using the Shapiro–Wilk test, and equality of variance using the Fisher test. Wherever normality and variance equality were confirmed, an unpaired Student's t-test was applied for the appropriate variables. Wherever one of the above two conditions was not validated, a Mann–Whitney test was performed. Regarding exclusion criteria, when appropriate, the distribution of the observed values and the definition of some of them as extreme values were tested using the ROUT method. Data analysis and statistical tests were achieved using the Prism8 software (GraphPad Software, San Diego, California, United States).

The results obtained from the 3-object recognition test were analysed using a mixed ANOVA model combining the repetition of exploring the objects over the 3 days of testing and the effects of the treatment (control vs HFHC). The same statistical procedure was used to assess the ability of rats to detect the object changes and the effects of the HFHC diet on days 3 and 4.

### Data availability

The datasets generated and analysed for this study are available from the corresponding author upon reasonable request.

Received: 27 November 2024; Accepted: 12 March 2025

## References

- Cholongitas, E. et al. Epidemiology of nonalcoholic fatty liver disease in Europe: A systematic review and meta-analysis. *Ann. Gastroenterol.* **34**, 404–414. <https://doi.org/10.20524/aog.2021.0604> (2021).
- Nagral, A. et al. Gender differences in nonalcoholic fatty liver disease. *Euroasian J. Hepatogastroenterol.* **12**, S19–s25. <https://doi.org/10.5005/jp-journals-10018-1370> (2022).
- Cherubini, A., Della Torre, S., Pelusi, S. & Valentini, L. Sexual dimorphism of metabolic dysfunction-associated steatotic liver disease. *Trends Molecular Med.* **30**, 1126–1136. <https://doi.org/10.1016/j.molmed.2024.05.013> (2024).
- Ratziu, V., Bellentani, S., Cortez-Pinto, H., Day, C. & Marchesini, G. A position statement on NAFLD/NASH based on the EASL 2009 special conference. *J. Hepatol.* **53**, 372–384. <https://doi.org/10.1016/j.jhep.2010.04.008> (2010).
- Rinella, M. E. et al. A multisociety Delphi consensus statement on new fatty liver disease nomenclature. *J. Hepatol.* **79**, 1542–1556. <https://doi.org/10.1016/j.jhep.2023.06.003> (2023).
- Basaranoglu, M. & Neuschwander-Tetri, B. A. Nonalcoholic fatty liver disease: Clinical features and pathogenesis. *Gastroenterol. Hepatol. (N Y)* **2**, 282–291 (2006).
- Long, M. T. et al. Nonalcoholic fatty liver disease and vascular function. *Arterioscl. Thrombosis Vascular Biol.* **35**, 1284–1291. <https://doi.org/10.1161/ATVBAHA.114.305200> (2015).
- Kim, D. et al. Depression is associated with non-alcoholic fatty liver disease among adults in the United States. *Aliment Pharmacol. Ther.* **50**, 590–598. <https://doi.org/10.1111/apt.15395> (2019).
- Weinstein, G. et al. Non-alcoholic fatty liver disease, liver fibrosis score and cognitive function in middle-aged adults: The Framingham Study. *Liver Int.* **39**, 1713–1721. <https://doi.org/10.1111/liv.14161> (2019).
- Medina-Julio, D. et al. From liver to brain: How MAFLD/MASLD impacts cognitive function. *Med. Sci. Monit.* **30**, e943417. <https://doi.org/10.12659/msm.943417> (2024).
- Kjaergaard, K. et al. Cognitive dysfunction in non-alcoholic fatty liver disease—current knowledge mechanisms and perspectives. *J. Clin. Med.* <https://doi.org/10.3390/jcm10040673> (2021).
- Veniaminova, E. et al. Prefrontal cortex inflammation and liver pathologies accompany cognitive and motor deficits following Western diet consumption in non-obese female mice. *Life Sci.* **241**, 117163. <https://doi.org/10.1016/j.lfs.2019.117163> (2020).
- Meroni, M., Longo, M., Paolini, E. & Dongiovanni, P. A narrative review about cognitive impairment in metabolic dysfunction-associated steatotic liver disease (MASLD): Another matter to face through a holistic approach. *J. Adv. Res.* **68**, 231–240. <https://doi.org/10.1016/j.jare.2024.02.007> (2025).
- Um, Y. J. et al. Sleep duration, sleep quality, and the development of nonalcoholic fatty liver disease: A cohort study. *Clin. Transl. Gastroenterol.* **12**, e00417. <https://doi.org/10.14309/ctg.0000000000000417> (2021).
- Taketani, H. et al. The association of insomnia with gastroesophageal reflux symptoms in biopsy-proven nonalcoholic fatty liver disease. *J. Gastroenterol.* **49**, 1163–1174. <https://doi.org/10.1007/s00535-013-0871-5> (2014).
- Balzano, T. et al. Histological features of cerebellar neuropathology in patients with alcoholic and nonalcoholic steatohepatitis. *J. Neuropathol. Exp. Neurol.* **77**, 837–845. <https://doi.org/10.1093/jnen/nly061> (2018).
- Balzano, T. et al. The cerebellum of patients with steatohepatitis shows lymphocyte infiltration, microglial activation and loss of purkinje and granular neurons. *Sci. Rep.* **8**, 3004. <https://doi.org/10.1038/s41598-018-21399-6> (2018).
- Kjærsgaard, K. et al. Cognitive dysfunction in early experimental metabolic dysfunction-associated steatotic liver disease is associated with systemic inflammation and neuroinflammation. *JHEP Rep.* **6**, 100992. <https://doi.org/10.1016/j.jhepr.2023.100992> (2024).
- Hadjihambi, A. et al. Partial MCT1 inactivation protects against diet-induced non-alcoholic fatty liver disease and the associated brain dysfunction. *J. Hepatol.* **78**, 180–190. <https://doi.org/10.1016/j.jhep.2022.08.008> (2023).
- Maciejewska, D. et al. Diet-induced rat model of gradual development of non-alcoholic fatty liver disease (NAFLD) with lipopolysaccharides (LPS) secretion. *Diagnostics (Basel)* <https://doi.org/10.3390/diagnostics9040205> (2019).
- Wang, Z. et al. The protective effects of the beta3 adrenergic receptor agonist BRL37344 against liver steatosis and inflammation in a rat model of high-fat diet-induced nonalcoholic fatty liver disease (NAFLD). *Mol. Med.* **26**, 54. <https://doi.org/10.1186/s10020-020-00164-4> (2020).
- Romestaing, C. et al. Long term highly saturated fat diet does not induce NASH in Wistar rats. *Nut. Metab. (Lond)* **4**, 4. <https://doi.org/10.1186/1743-7075-4-4> (2007).
- Donnelly, K. L. et al. Sources of fatty acids stored in liver and secreted via lipoproteins in patients with nonalcoholic fatty liver disease. *J. Clin. Invest.* **115**, 1343–1351. <https://doi.org/10.1172/JCI23621> (2005).
- Asai, A. et al. Dissociation of hepatic insulin resistance from susceptibility of nonalcoholic fatty liver disease induced by a high-fat and high-carbohydrate diet in mice. *Am. J. Physiol. Gastrointest. Liver Physiol.* **306**, G496–504. <https://doi.org/10.1152/ajpgi.00291.2013> (2014).
- de Assis, A. M. et al. High fat and highly thermolyzed fat diets promote insulin resistance and increase DNA damage in rats. *Exp. Biol. Med. (Maywood)* **234**, 1296–1304. <https://doi.org/10.3181/0904-RM-126> (2009).
- Fraulob, J. C., Ogg-Diamantino, R., Fernandes-Santos, C., Aguila, M. B. & Mandarim-de-Lacerda, C. A. A mouse model of metabolic syndrome: Insulin resistance, fatty liver and non-alcoholic fatty pancreas disease (NAFPD) in C57BL/6 mice fed a high fat diet. *J. Clin. Biochem. Nutr.* **46**, 212–223. <https://doi.org/10.3164/jcbs.09-83> (2010).
- Grundleger, M. L. & Thenen, S. W. Decreased insulin binding, glucose transport, and glucose metabolism in soleus muscle of rats fed a high fat diet. *Diabetes* **31**, 232–237. <https://doi.org/10.2337/diab.31.3.232> (1982).
- Yang, H. et al. Circadian disturbances by altering the light–dark cycle negatively affects hematopoietic function of bone marrow in mice. *FASEB J.* **38**, e23565. <https://doi.org/10.1096/fj.2023022338> (2024).
- Cuesta, M., Clesse, D., Pevet, P. & Challet, E. From daily behavior to hormonal and neurotransmitters rhythms: Comparison between diurnal and nocturnal rat species. *Horm. Behav.* **55**, 338–347. <https://doi.org/10.1016/j.yhbeh.2008.10.015> (2009).
- Perez-Diaz-Del-Campo, N. et al. Role of circadian clock on the pathogenesis and lifestyle management in non-alcoholic fatty liver disease. *Nutrients* <https://doi.org/10.3390/nu14235053> (2022).
- de Assis, L. V. M., Demir, M. & Oster, H. Nonalcoholic steatohepatitis disrupts diurnal liver transcriptome rhythms in mice. *Cell Mol. Gastroenterol. Hepatol.* **16**, 341–354. <https://doi.org/10.1016/j.jcmgh.2023.05.008> (2023).
- Wang, F. et al. Night shift work and abnormal liver function: is non-alcohol fatty liver a necessary mediator?. *Occup. Environ. Med.* **76**, 83–89. <https://doi.org/10.1136/oemed-2018-105273> (2019).
- Liu, H. et al. The association between sleep duration, quality, and nonalcoholic fatty liver disease: A cross-sectional study. *Open Med. (Wars)* <https://doi.org/10.1515/med-2023-0670> (2023).
- Tissot, C. et al. Neuroinflammation is associated with non-REM sleep reduction in individuals without dementia. *Alzheimer's Dementia* **16**, e046636. <https://doi.org/10.1002/alz.046636> (2020).
- Manchanda, S., Singh, H., Kaur, T. & Kaur, G. Low-grade neuroinflammation due to chronic sleep deprivation results in anxiety and learning and memory impairments. *Mol. Cell. Biochem.* **449**, 63–72. <https://doi.org/10.1007/s11010-018-3343-7> (2018).
- Friedman, N. P. & Robbins, T. W. The role of prefrontal cortex in cognitive control and executive function. *Neuropsychopharmacology* **47**, 72–89. <https://doi.org/10.1038/s41386-021-01132-0> (2022).

37. Hong, J., Lozano, D. E., Beier, K. T., Chung, S. & Weber, F. Prefrontal cortical regulation of REM sleep. *Nat. Neurosci.* **26**, 1820–1832. <https://doi.org/10.1038/s41593-023-01398-1> (2023).
38. Benarroch, E. What is the involvement of the cerebellum during sleep?. *Neurology* **100**, 572–577. <https://doi.org/10.1212/WNL.000000000000207161> (2023).
39. Hoogland, I. C., Houbolt, C., van Westerloo, D. J., van Gool, W. A. & van de Beek, D. Systemic inflammation and microglial activation: Systematic review of animal experiments. *J. Neuroinflamm.* **12**, 114. <https://doi.org/10.1186/s12974-015-0332-6> (2015).
40. Guzman-Ruiz, M. A. et al. Circadian modulation of microglial physiological processes and immune responses. *Glia* **71**, 155–167. <https://doi.org/10.1002/glia.24261> (2023).
41. Hsu, J. C. et al. Sleep deprivation inhibits expression of NADPH-d and NOS while activating microglia and astroglia in the rat hippocampus. *Cells Tissues Organs*. **173**, 242–254. <https://doi.org/10.1159/000070380> (2003).
42. Cheadle, L. et al. Sensory experience engages microglia to shape neural connectivity through a non-phagocytic mechanism. *Neuron* <https://doi.org/10.1016/j.neuron.2020.08.002> (2020).
43. Sonar, S. & Lal, G. Role of tumor necrosis factor superfamily in neuroinflammation and autoimmunity. *Front. Immun.* <https://doi.org/10.3389/fimmu.2015.00364> (2015).
44. Paolicelli, R. C., Bisht, K. & Tremblay, M. -È. Fractalkine regulation of microglial physiology and consequences on the brain and behavior. *Front. Cell. Neurosci.* <https://doi.org/10.3389/fncel.2014.00129> (2014).
45. Dabrowski, A., Terauchi, A., Strong, C. & Umemori, H. Distinct sets of FGF receptors sculpt excitatory and inhibitory synaptogenesis. *Development* **142**, 1818–1830. <https://doi.org/10.1242/dev.115568> (2015).
46. Labandeira-Garcia, J. L., Costa-Besada, M. A., Labandeira, C. M., Villar-Cheda, B. & Rodriguez-Perez, A. I. Insulin-like growth factor-1 and neuroinflammation. *Front. Aging. Neurosci.* **9**, 365. <https://doi.org/10.3389/fnagi.2017.00365> (2017).
47. Terashima, T. et al. Stem cell factor induces polarization of microglia to the neuroprotective phenotype in vitro. *Heliyon* **4**, e00837. <https://doi.org/10.1016/j.heliyon.2018.e00837> (2018).
48. Boato, F. et al. Interleukin-1 beta and neurotrophin-3 synergistically promote neurite growth in vitro. *J. Neuroinflamm.* **8**, 183. <https://doi.org/10.1186/1742-2094-8-183> (2011).
49. Zhao, P. et al. Fetuin-A alleviates neuroinflammation against traumatic brain injury-induced microglial necroptosis by regulating Nrf-2/HO-1 pathway. *J. Neuroinflamm.* **19**, 269. <https://doi.org/10.1186/s12974-022-02633-5> (2022).
50. McAlpine, C. S. et al. Astrocytic interleukin-3 programs microglia and limits Alzheimer’s disease. *Nature* **595**, 701–706. <https://doi.org/10.1038/s41586-021-03734-6> (2021).
51. Tan, Q. et al. The interaction of lipocalin-2 and astrocytes in neuroinflammation: mechanisms and therapeutic application. *Front. Immunol.* **15**, 1358719. <https://doi.org/10.3389/fimmu.2024.1358719> (2024).
52. Gulyassy, P. et al. The effect of sleep deprivation and subsequent recovery period on the synaptic proteome of rat cerebral cortex. *Mol. Neurobiol.* **59**, 1301–1319. <https://doi.org/10.1007/s12035-021-02699-x> (2022).

## Acknowledgements

The authors are very grateful to the staff of the NGERE Laboratory. They would like to thank (i) Manon Jeandel, Arnaud Michel, Noémie Marchal, Jean-Marc Alberto and Rémy Umoret for their occasional help in carrying out the animal experimentation protocols, (ii) Hugo Jadot, Océane Villaume and Assmaa Tanji as trainees for their contribution to the analysis of specimens and (iii) the “Animalerie Campus Biologie Santé”, Université de Lorraine, for its expertise in animal welfare and experimentation. We would also like to thank Pr. Rosa-Maria Guéant Rodriguez and the medical biology laboratory of the “CHRU” of Nancy for lipid and enzymatic measurements of plasma. We would also like to thank Dr Clément Kebbabi of the Laboratoire National de Santé du Luxembourg for lipid measurements of the liver and Dr Fatima Descles of the IBBL for scanning the liver and pancreas slides. We also wish to thank H2P2 facilities (Histo Pathologie Haute Precision) (Biosit SFR UMS CNRS 3480 Inserm 018); notably Roselyne Viel, Gevorg Ghukasyan and Pascale Bellaud for their technical assistance in histopathology experiments. The graphical abstract as well as Figs. 1, 2, 3, 4, 5, 6, 7 and 8 were made with Biorender.com using the agreement number: XJ27EVT4A – Grova, N.

## Author contributions

PH.G.: Methodology, Resources, Investigation, Validation, Software, Writing – 70% Original Draft, Writing—Review & Editing; J.P.: Methodology, Investigation, Writing—Review & Editing; B.Y.: Investigation, Review & Editing; C.M.: Investigation, Review & Editing; A.H.: Investigation, Review & Editing; M.C.: Investigation, Review & Editing; I.G.: Investigation, Review & Editing; D.L.G.: Conceptualization, Review & Editing; S.B.: Investigation; B.P.: Review & Editing; D.M.: Review & Editing; O.S.: Conceptualization, Review & Editing; H.S.: Conceptualization, Supervision, Visualization, Methodology, Resources, Review & Editing. N.G.: Project administration, Conceptualization, Supervision, Visualization, Methodology, Investigation, Resources, Validation, Writing – 30% Original Draft, Review & Editing.

## Funding

This work was supported by the “Fondation pour la recherche médicale” (FRM-ENV202109013686). It has no implication in the study design, in the collection, analysis and interpretation of data, in the writing of the report and in the decision to submit the article for publication. We also acknowledge the “Ministère de l’Enseignement supérieur et de la Recherche” in France for the continued support.

## Declarations

## Competing interests

The authors declare no competing interests.

## Additional information

**Supplementary Information** The online version contains supplementary material available at <https://doi.org/10.1038/s41598-025-94234-4>.

**Correspondence** and requests for materials should be addressed to N.G.

**Reprints and permissions information** is available at [www.nature.com/reprints](http://www.nature.com/reprints).

**Publisher's note** Springer Nature remains neutral with regard to jurisdictional claims in published maps and institutional affiliations.

**Open Access** This article is licensed under a Creative Commons Attribution-NonCommercial-NoDerivatives 4.0 International License, which permits any non-commercial use, sharing, distribution and reproduction in any medium or format, as long as you give appropriate credit to the original author(s) and the source, provide a link to the Creative Commons licence, and indicate if you modified the licensed material. You do not have permission under this licence to share adapted material derived from this article or parts of it. The images or other third party material in this article are included in the article's Creative Commons licence, unless indicated otherwise in a credit line to the material. If material is not included in the article's Creative Commons licence and your intended use is not permitted by statutory regulation or exceeds the permitted use, you will need to obtain permission directly from the copyright holder. To view a copy of this licence, visit <http://creativecommons.org/licenses/by-nc-nd/4.0/>.

© The Author(s) 2025